

Modeling the uncertainty on the covariance matrix for probabilistic forecast reconciliation

Chiara Carrara^{a,b,*}, Dario Azzimonti^b, Giorgio Corani^b, Lorenzo Zambon^b

^a*University of Pavia*
^b*SUPSI, Istituto Dalle Molle di Studi sull'Intelligenza Artificiale (IDSIA)*

Abstract

In forecast reconciliation, the covariance matrix of the base forecasts errors plays a crucial role. Typically, this matrix is estimated, and then treated as known. In contrast, we propose a Bayesian reconciliation model that accounts for the uncertainty in the estimation of the covariance matrix. This leads to a reconciled predictive distribution that follows a multivariate t-distribution, obtained in closed-form, rather than a multivariate Gaussian. We evaluate our method on three tourism-related datasets, including a new publicly available dataset. Empirical results show that our approach consistently improves prediction intervals compared to Gaussian reconciliation.

Keywords: Probabilistic forecast reconciliation, Covariance matrix uncertainty, Tourism forecasting, Bayesian modeling

1. Introduction

Hierarchical time series are collections of time series that adhere to a set of linear constraints. To ensure that the forecasts are *coherent*, i.e., that they respect the constraints, a common approach is to first generate incoherent base forecasts and then to reconcile them. The state-of-the art reconciliation method is MinT, which is optimal with respect to the mean squared error (Wickramasuriya, Athanasopoulos & Hyndman, 2019) and to the log score (Wickramasuriya, 2024), assuming the covariance matrix of the errors of the base forecasts to be known. In practice, however, the covariance matrix is estimated from the in-sample residuals and it is, thus, affected by the estimation error. A common approach to estimate the covariance matrix is via shrinkage (Schäfer & Strimmer, 2005), which offers improved accuracy over the sample covariance.

Yet, the estimation error on the covariance matrix affects the accuracy of the reconciled forecasts (Pritularga, Svetunkov & Kourentzes, 2021). Current reconciliation algorithms (Wickramasuriya et al., 2019; Corani, Azzimonti, Augusto & Zaffalon, 2020; Wickramasuriya, 2024; Yang, Athanasopoulos, Hyndman & Panagiotelis, 2024; Girolimetto, Athanasopoulos, Di Fonzo & Hyndman, 2024) use a point estimate of the covariance matrix, without considering the uncertainty in the estimation. In Bayesian inference, the predictive distribution accounts for the uncertainty about the parameters (Gelman, Carlin, Stern, Dunson, Vehtari & Rubin, 2013, Chap. 1.3), yielding a more reliable assessment of uncertainty. We thus propose a Bayesian reconciliation approach that accounts for the uncertainty of the covariance matrix. We call our method *t-Rec*, as the resulting reconciled distribution is a multivariate t.

In order to set the prior distribution on the covariance matrix \mathbf{W} , we use the covariance of the in-sample residuals of simple forecasting methods such as naive and seasonal naive. We obtain the posterior distribution of \mathbf{W} by updating the prior with the likelihood of the in-sample residuals of the base forecasts, which we assume to be Gaussian given \mathbf{W} . We then analytically derive the posterior predictive distribution of the base forecasts, which is a multivariate t. This distribution is however incoherent and needs to be reconciled. We adopt reconciliation via conditioning (Corani et al., 2020; Zambon, Azzimonti & Corani, 2024b). We perform the conditioning in closed form thanks to the closure of the multivariate t under linear transfor-

*Corresponding author
 Email address: chiara.carrara03@universitadipavia.it (Chiara Carrara)

mations and conditioning. Thus, we analytically obtain the coherent predictive distribution, which is still a multivariate t , with a small computation overhead compared to probabilistic Gaussian reconciliation. On the point forecasts t -*Rec* provides practically no improvement over probabilistic Gaussian reconciliation (Zambon et al., 2024b; Wickramasuriya, 2024); instead, it consistently improves the prediction intervals, thanks to heavier tails of the predictive distribution. Indeed, Gaussian reconciliation always reduces (Zambon, Agosto, Giudici & Corani, 2024a) the length of the prediction intervals compared to the base forecasts. Instead, the prediction intervals of t -*Rec* can also be larger than those of the base forecasts; this happens especially if the base forecasts are largely incoherent. This, arguably, can yield a better assessment of uncertainty.

The paper is structured as follows: in Sect. 2 we introduce the notation, we recall the concepts of probabilistic reconciliation and MinT reconciliation; in Sect. 3 we analytically derive t -*Rec* and we discuss its specifications; in Sect. 4 we show how the model behaves on a minimal hierarchy; in Sect. 5 we report empirical results on real datasets; in Sect. 6 we present our conclusions.

2. Probabilistic reconciliation

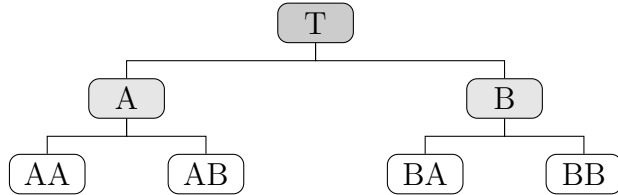


Figure 1: Hierarchy with 4 bottom and 3 upper time series.

Fig. 1 is an example of hierarchical time series. It could represent the total visitors of a country (T), disaggregated by zones (A, B) and regions (AA, AB, BA, BB), so that:

$$T = A + B, \quad A = AA + AB, \quad B = BA + BB.$$

At any time t , the hierarchical constraints between time series are given by:

$$\mathbf{u}_t = \mathbf{Ab}_t, \tag{1}$$

where $\mathbf{A} \in \mathbb{R}^{n_u \times n_b}$ is the *aggregation matrix*, which is made of 0 and 1 and specifies how the *bottom* time series $\mathbf{b}_t \in \mathbb{R}^{n_b}$ aggregate to the *upper* time series $\mathbf{u}_t \in \mathbb{R}^{n_u}$. The *summing matrix* $\mathbf{S} \in \mathbb{R}^{n \times n_b}$, defined as:

$$\mathbf{S} = \begin{bmatrix} \mathbf{A} \\ \mathbf{I}_{n_b \times n_b} \end{bmatrix},$$

encodes the hierarchy via $\mathbf{y}_t = \mathbf{Sb}_t$, where $\mathbf{y}_t = [\mathbf{u}_t^T, \mathbf{b}_t^T]^T \in \mathbb{R}^n$. Although we adopt the formulation based on the summation matrix, our discussion applies also to the more general linearly constrained time series framework of Girolimetto & Di Fonzo (2024).

We consider probabilistic forecasts in the form of a joint predictive distribution $\hat{\pi}$ over \mathbb{R}^n . The forecast distribution $\hat{\pi}$ should be *coherent*, i.e., it should give positive probability only to regions of points that satisfy the hierarchical constraints. This means that the support of $\hat{\pi}$ should lie on the *coherent subspace* \mathcal{S} , defined as $\mathcal{S} := \{\mathbf{y} \in \mathbb{R}^n \text{ such that } \mathbf{y} = \mathbf{Sb}\}$, so that any sample drawn from $\hat{\pi}$ satisfies the hierarchical constraints. The goal of probabilistic reconciliation is to find a coherent reconciled forecast distribution $\tilde{\pi}$. For a more detailed discussion on probabilistic reconciliation, we refer to Panagiotelis, Gamakumara, Athanasopoulos & Hyndman (2023); Zambon et al. (2024b).

MinT reconciliation. The Minimum Trace (MinT) reconciliation method was initially introduced for the reconciliation of point forecasts by Wickramasuriya et al. (2019). Given the h -step ahead base point forecasts $\hat{\mathbf{y}}_{t+h|t}$, computed at time t for time $t+h$, the reconciled point forecasts $\tilde{\mathbf{y}}_{t+h|t}$ are obtained by projecting $\hat{\mathbf{y}}_{t+h|t}$ on the coherent subspace \mathcal{S} :

$$\tilde{\mathbf{y}}_{t+h|t} = \mathbf{S}\mathbf{P}_h\hat{\mathbf{y}}_{t+h|t}, \quad (2)$$

where $\mathbf{P}_h = (\mathbf{S}^T \mathbf{W}_h^{-1} \mathbf{S})^{-1} \mathbf{S}^T \mathbf{W}_h^{-1}$, and \mathbf{W}_h is the covariance matrix of the h -step ahead base forecast errors. Assuming that the base forecasts $\hat{\mathbf{y}}_{t+h|t}$ are unbiased and that the matrix \mathbf{W}_h is known, the reconciled point forecasts $\tilde{\mathbf{y}}_{t+h|t}$ are optimal in terms of the Mean Squared Error (MSE).

MinT was later extended to the probabilistic case by projecting on \mathcal{S} the entire forecast distribution $\tilde{\pi}$ (Panagiotelis et al., 2023). If the joint base forecast distribution is Gaussian, i.e., $\tilde{\pi} = \text{MVN}(\hat{\mathbf{y}}_{t+h|t}, \mathbf{W}_h)$, the reconciled distribution is also Gaussian:

$$\tilde{\pi} = \text{MVN}(\tilde{\mathbf{y}}_{t+h|t}, \tilde{\mathbf{W}}_h),$$

where $\tilde{\mathbf{y}}_{t+h|t}$ is given by Eq. (2) and $\tilde{\mathbf{W}}_h = \mathbf{S}\mathbf{P}_h\mathbf{W}_h\mathbf{P}_h^T\mathbf{S}^T$. In the Gaussian case, $\tilde{\pi}$ is optimal with respect to the log-score (Wickramasuriya, 2024).

Probabilistic reconciliation via conditioning. An alternative approach to probabilistic reconciliation derives the reconciled distribution by conditioning the joint base forecast distribution on the hierarchical constraints (Corani et al., 2020; Zambon et al., 2024b). Given $\hat{\mathbf{Y}} = [\hat{\mathbf{U}}^T, \hat{\mathbf{B}}^T]^T$, a random vector distributed as the h -step ahead base forecast distribution $\hat{\pi}$, the reconciled distribution of the bottom series is given by

$$\tilde{\mathbf{B}} \sim \hat{\mathbf{B}} \mid (\hat{\mathbf{U}} - \mathbf{A}\hat{\mathbf{B}} = 0),$$

and it can be extended to the entire hierarchy via $\tilde{\mathbf{Y}} = \mathbf{S}\tilde{\mathbf{B}}$ (Zambon et al., 2024b). If the base forecast distribution is jointly Gaussian, the solution of reconciliation via conditioning coincides with MinT (Corani et al., 2020; Zambon, Azzimonti, Rubattu & Corani, 2024c). Reconciliation via conditioning can be interpreted as slicing the incoherent joint density over the coherent subspace \mathcal{S} .

Estimation of \mathbf{W}_1 . For $h = 1$, \mathbf{W}_1 is typically estimated as the covariance matrix of the in-sample residuals. Empirically, the most effective choice (Wickramasuriya et al., 2019; Panagiotelis, Athanasopoulos, Gamakumara & Hyndman, 2021; Di Fonzo & Girolimetto, 2024) appears to be the shrinkage estimator (Schäfer & Strimmer, 2005):

$$\hat{\mathbf{W}}_1 = (1 - \lambda_{\text{shrink}})\hat{\Sigma}_1 + \lambda_{\text{shrink}}\hat{\mathbf{D}}_1, \quad (3)$$

where $\hat{\Sigma}_1$ is the sample covariance matrix of the 1-step ahead residuals, $\hat{\mathbf{D}}_1$ is the diagonal matrix of the sample variances, and $\lambda_{\text{shrink}} \in [0, 1]$ is the optimal shrinkage parameter. Double shrinkage approaches have also been proposed (Wickramasuriya, 2017, Chap. 4.3.3; Carrara, Zambon, Azzimonti & Corani, 2025), but they either offer limited improvements or incur in significant computational cost. In what follows, we denote by *MinT* the MinT reconciliation method with the shrinkage estimator $\hat{\mathbf{W}}_1$.

Estimation of \mathbf{W}_h . There is no standard method for estimating \mathbf{W}_h for $h > 1$. Wickramasuriya et al. (2019) assume $\mathbf{W}_h = k_h \mathbf{W}_1$ for some constant k_h , which does not need to be estimated to compute the reconciled point forecasts $\tilde{\mathbf{y}}_{t+h|t}$. Yet, in a probabilistic framework, k_h is needed to compute the reconciled variance; some heuristic strategies have been proposed by Corani et al. (2020). Alternative approaches are given by Girolimetto et al. (2024), where \mathbf{W}_h is estimated using multi-step residuals. Our method can be applied with any choice of \mathbf{W}_h ; in our experiments, we only consider the case $h = 1$. From now on, we drop the h subscript for ease of notation.

3. Probabilistic reconciliation modeling the uncertainty on \mathbf{W}

We propose a Bayesian approach to model the uncertainty on \mathbf{W} . We set a prior on \mathbf{W} and update it using the in-sample residuals. We then compute the posterior predictive distribution by marginalizing the posterior joint distribution over \mathbf{W} . The resulting incoherent predictive distribution is a multivariate t, which we reconcile via conditioning, obtaining a coherent multivariate t in closed form. We call our method *t-Rec*.

Prior of \mathbf{W} . We adopt an Inverse-Wishart (IW) prior distribution for \mathbf{W} :

$$\mathbf{W} \sim \text{IW}(\Psi_0, \nu_0), \quad (4)$$

where $\Psi_0 \in \mathbb{R}^{n \times n}$ is the scale parameter and $\nu_0 \in \mathbb{R}$ is the degree of freedom. The Inverse-Wishart is a distribution defined on the space of positive-definite matrices, with density

$$\text{IW}(\mathbf{W}; \Psi_0, \nu_0) = \frac{|\Psi_0|^{\frac{\nu_0}{2}}}{2^{\frac{n\nu_0}{2}} \Gamma_n\left(\frac{\nu_0}{2}\right)} |\mathbf{W}|^{-\frac{\nu_0+n+1}{2}} \exp\left(-\frac{\text{tr}(\Psi_0 \mathbf{W}^{-1})}{2}\right),$$

where $|\cdot|$ denotes the determinant, tr the trace, and Γ_n the multivariate gamma function (Gupta & Nagar, 2018).

Likelihood of the residuals. As in Corani et al. (2020); Wickramasuriya (2024), we assume that, conditionally on \mathbf{W} , the base predictive distribution is Gaussian with covariance matrix \mathbf{W} , and that the base forecasts are unbiased. The in-sample residuals $\mathbf{r}_1, \dots, \mathbf{r}_T$, defined as $\mathbf{r}_j = \hat{\mathbf{y}}_j - \mathbf{y}_j$ for $j = 1, \dots, T$, are thus assumed to be independent and identically distributed (IID) as a multivariate Gaussian with zero mean and covariance matrix \mathbf{W} :

$$\mathbf{r}_1, \dots, \mathbf{r}_T \mid \mathbf{W} \stackrel{\text{IID}}{\sim} \text{MVN}(\mathbf{0}, \mathbf{W}). \quad (5)$$

Posterior of \mathbf{W} . Thanks to conjugacy (Gelman et al., 2013, Chap. 3.6), the posterior distribution of \mathbf{W} is still Inverse-Wishart:

$$\mathbf{W} \mid \mathbf{R} \sim \text{IW}(\mathbf{W}; \Psi', \nu'), \quad (6)$$

with parameters $\nu' = \nu_0 + T$ and $\Psi' = \Psi_0 + \mathbf{R}\mathbf{R}^T$, where $\mathbf{R} := [\mathbf{r}_1 \dots \mathbf{r}_T] \in \mathbb{R}^{n \times T}$ is the matrix of the in-sample residuals.

Multivariate t base predictive distribution. The incoherent posterior predictive distribution of the base forecasts is a multivariate t-distribution (Gelman et al., 2013, Chap. 3.6), obtained by computing the posterior joint distribution $\hat{\pi}(\mathbf{y}, \mathbf{W} \mid \mathbf{R})$ and then marginalizing out \mathbf{W} :

$$\begin{aligned} \hat{\pi}(\mathbf{y} \mid \mathbf{R}) &= \int \hat{\pi}(\mathbf{y}, \mathbf{W} \mid \mathbf{R}) d\mathbf{W} \\ &= \int \hat{\pi}(\mathbf{y} \mid \mathbf{W}) \pi(\mathbf{W} \mid \mathbf{R}) d\mathbf{W} \\ &= \int \text{MVN}(\mathbf{y}; \hat{\mathbf{y}}, \mathbf{W}) \text{IW}(\mathbf{W}; \Psi', \nu') d\mathbf{W} \\ &= \text{mt}\left(\mathbf{y}; \hat{\mathbf{y}}, \frac{1}{\nu' - n + 1} \Psi', \nu' - n + 1\right). \end{aligned} \quad (7)$$

Reconciliation. The multivariate t-distribution is closed under affine transformations and conditioning (Kotz & Nadarajah, 2004). Hence, we obtain analytically the reconciled distribution via conditioning, as stated in the following theorem, which we prove in Appendix A.

Theorem 1. *Given a hierarchy specified by Eq. (1), and under the model of Eq. (4) and Eq. (5), the reconciled distribution via conditioning of the bottom time series is a multivariate t-distribution:*

$$\tilde{\mathbf{B}} \sim \text{mt}\left(\tilde{\mathbf{b}}, \tilde{\Sigma}_B, \tilde{\nu}\right), \quad (8)$$

where

$$\tilde{\mathbf{b}} = \hat{\mathbf{b}} + \left(\Psi'_{UB}^T - \Psi'_B \mathbf{A}^T\right) \mathbf{Q}^{-1}(\mathbf{A}\hat{\mathbf{b}} - \hat{\mathbf{u}}), \quad (9)$$

$$\tilde{\Sigma}_B = C \left[\Psi'_B - \left(\Psi'_{UB}^T - \Psi'_B \mathbf{A}^T\right) \mathbf{Q}^{-1} \left(\Psi'_{UB}^T - \Psi'_B \mathbf{A}^T\right)^T \right], \quad (10)$$

$$\tilde{\nu} = \nu' - n_b + 1, \quad (11)$$

and

$$C = \frac{1 + (\mathbf{A}\hat{\mathbf{b}} - \hat{\mathbf{u}})^T \mathbf{Q}^{-1} (\mathbf{A}\hat{\mathbf{b}} - \hat{\mathbf{u}})}{\tilde{\nu}},$$

$$\mathbf{Q} = \Psi'_U - \Psi'_{UB} \mathbf{A}^T - \mathbf{A} \Psi'_{UB}^{-T} + \mathbf{A} \Psi'_B \mathbf{A}^T.$$

Theorem 1 provides the reconciled distribution for the bottom-level time series. The reconciled distribution for the entire hierarchy is a multivariate \mathbf{t} with mean $\tilde{\mathbf{y}} = \mathbf{S}\tilde{\mathbf{b}}$, scale matrix $\mathbf{S}\tilde{\Sigma}_B\mathbf{S}^T$, and degrees of freedom $\tilde{\nu}$.

3.1. Parameters of the prior distribution

We now discuss our choices for the scale matrix Ψ_0 and the degree of freedom ν_0 of the Inverse-Wishart prior.

Scale matrix. $\Psi_0 \in \mathbb{R}^{n \times n}$ is a positive definite matrix, proportional to the prior mean Ψ of the IW distribution via $\Psi_0 = (\nu_0 - n - 1)\Psi$. We set Ψ to be the shrinkage estimate of the covariance matrix of the residuals from either the naive or the seasonal naive method. The choice between these two methods is based on the outcome of the KPSS seasonality test, implemented in the `forecast` package (Hyndman & Khandakar, 2008). We thus use the covariance of the residuals of such simple methods as prior information for the covariance of the residuals of the more complex models which are later used to generate the base forecasts.

Degree of freedom. The parameter ν_0 represents the strength of belief in the prior information: a higher value indicates stronger confidence in the prior. We set $\nu_0 \in \mathbb{R}$ by maximizing the out-of-sample performance, estimated via Bayesian leave-one-out (LOO) cross-validation (Vehtari, Gelman & Gabry, 2017):

$$\begin{aligned} \nu_0 &:= \arg \max_{\nu \in [n+2, 5n]} \log \left(\prod_{i=1}^T \pi(\mathbf{r}_i | \mathbf{R}_{-i}) \right) \\ &= \arg \max_{\nu \in [n+2, 5n]} \sum_{i=1}^T \log \left(\text{mt} \left(\mathbf{r}_i; 0, \frac{1}{\nu + T - n} (\Psi_0 + \mathbf{R}_{-i} \mathbf{R}_{-i}^T), \nu + T - n \right) \right), \end{aligned} \quad (12)$$

where $\mathbf{R}_{-i} \in \mathbb{R}^{n \times (T-1)}$ is the matrix of the in-sample residuals without the column \mathbf{r}_i , and $\pi(\mathbf{r}_i | \mathbf{R}_{-i})$ is the posterior predictive density of the residuals \mathbf{r}_i , given the observations \mathbf{R}_{-i} ; the derivation of Eq. (12) is analogous to that of Eq. (7). The LOO approach is tenable since the residuals $\mathbf{r}_1, \dots, \mathbf{r}_T$ can be generally assumed to be IID (Svetunkov, 2023, Chap. 1.4.1). We restrict the search for the optimal value of ν_0 to the interval $[n+2, 5n]$, since the expected value of the IW prior is not defined for $\nu_0 < n+2$. The upper bound $\nu_0 = 5n$ is sufficiently large such that, in our experiments, the optimal ν_0 is consistently below it.

A naive evaluation of the objective function in Eq. (12) is computationally expensive as it requires the inversion of the T matrices $\Psi_0 + \mathbf{R}_{-i} \mathbf{R}_{-i}^T$, for $i = 1, \dots, T$. However, since these matrices are rank-1 updates of the same matrix: $\Psi_0 + \mathbf{R}_{-i} \mathbf{R}_{-i}^T = \Psi_0 + \mathbf{R} \mathbf{R}^T - \mathbf{r}_i \mathbf{r}_i^T$, we use the Sherman-Morrison formula (Sherman & Morrison, 1950) to obtain

$$(\Psi_0 + \mathbf{R}_{-i} \mathbf{R}_{-i}^T)^{-1} = (\Psi_0 + \mathbf{R} \mathbf{R}^T)^{-1} + \left(1 + \mathbf{r}_i^T (\Psi_0 + \mathbf{R} \mathbf{R}^T)^{-1} \mathbf{r}_i \right)^{-1} (\Psi_0 + \mathbf{R} \mathbf{R}^T)^{-1} \mathbf{r}_i \mathbf{r}_i^T (\Psi_0 + \mathbf{R} \mathbf{R}^T)^{-1}.$$

We thus compute only once the inverse of the matrix $\Psi_0 + \mathbf{R} \mathbf{R}^T$, achieving a significant speed-up. The optimization of ν is performed using the `nloptr` R package (Johnson, 2008). In our most computationally expensive experiment ($n = 111$, $T = 60$), the optimization requires less than 0.5 s on a standard laptop.

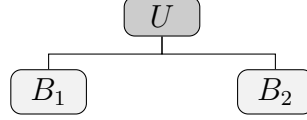


Figure 2: Hierarchy with one upper and two bottom time series.

4. Application to a minimal hierarchy

We compare *t-Rec* and *MinT* on the minimal hierarchy of Fig. 2. In this setting, the reconciled bottom and upper distribution are multivariate t and univariate t:

$$\tilde{\mathbf{B}} \sim \text{mt} \left(\tilde{\mathbf{b}}, \tilde{\boldsymbol{\Sigma}}_B, \tilde{\nu} \right), \quad \tilde{U} \sim t \left(\tilde{u}, \tilde{\sigma}_u, \tilde{\nu} \right), \quad (13)$$

where

$$\begin{aligned} \tilde{\nu} &= \nu' - 1, \\ \tilde{\mathbf{b}} &= \begin{bmatrix} \left(1 - \frac{g_1}{Q}\right) \hat{b}_1 + \frac{g_1}{Q} \left(\hat{u} - \hat{b}_2\right) \\ \left(1 - \frac{g_2}{Q}\right) \hat{b}_2 + \frac{g_2}{Q} \left(\hat{u} - \hat{b}_1\right) \end{bmatrix}, \quad \tilde{u} = \left(1 - \frac{g_u}{Q}\right) \hat{u} + \frac{g_u}{Q} \left(\hat{b}_1 + \hat{b}_2\right), \end{aligned} \quad (14)$$

$$\tilde{\boldsymbol{\Sigma}}_B = C \begin{bmatrix} \Psi'_1 - \frac{g_1^2}{Q} & \Psi'_{1,2} - \frac{g_1 g_2}{Q} \\ \Psi'_{1,2} - \frac{g_1 g_2}{Q} & \Psi'_2 - \frac{g_2^2}{Q} \end{bmatrix}, \quad \tilde{\sigma}_u^2 = C \left(\Psi'_u - \frac{g_u^2}{Q} \right), \quad (15)$$

and

$$\begin{aligned} C &= \frac{1}{\tilde{\nu}} \left(1 + \frac{(\hat{b}_1 + \hat{b}_2 - \hat{u})^2}{Q} \right), & Q &= g_1 + g_2 + g_u, \\ g_1 &= (\Psi'_1 + \Psi'_{1,2}) - \Psi'_{u,1}, & \Psi' &= \begin{bmatrix} \Psi'_u & \Psi'_{u,1} & \Psi'_{u,2} \\ \Psi'_{u,1} & \Psi'_1 & \Psi'_{1,2} \\ \Psi'_{u,2} & \Psi'_{1,2} & \Psi'_2 \end{bmatrix}. \end{aligned}$$

As in the Gaussian case (Corani et al., 2020; Hollyman, Petropoulos & Tipping, 2021; Zambon et al., 2024a), the reconciled point forecasts (Eq. (14)) are a combination of the base point forecasts; for example, the reconciled upper mean \tilde{u} is a convex combination of \hat{u} and $\hat{b}_1 + \hat{b}_2$.

However, there is an important difference in the reconciled prediction intervals. In the Gaussian case, the width of the prediction intervals always decreases after reconciliation since the reconciled variance is smaller than the variance of the base forecasts (Zambon et al., 2024a). In contrast, the prediction intervals of *t-Rec* can become wider than those of the base forecasts in case of large incoherence, defined as $|\mathbf{Ab} - \hat{u}|$; indeed, the scale parameters in Eq. (15) depend on the incoherence through the term C .

4.1. Simulations

We compare the prediction intervals of *MinT* and *t-Rec* using simulated time series. We run 1000 simulations, in which we simulate the time series, compute the base forecasts, and reconcile them. As in Wickramasuriya et al. (2019), we simulate the two bottom series as a structural time series model with trend, seasonality and correlated errors. The seasonality is set to 4, and the training length to 12. More details are reported in Appendix B. We obtain the upper series as the sum of the bottom series. We introduce model misspecification by computing the base forecasts with the ets model with additive noise from the R package `forecast` (Hyndman & Khandakar, 2008).

We define the *relative width* as the ratio between the width of the reconciled prediction interval and that of the base forecast. In Fig. 3, we show the distribution of the relative width of the 95% prediction intervals of *MinT* and *t-Rec*. The prediction intervals of *MinT* are always narrower than those of the base forecasts; indeed, the relative width is upper-bounded by 1. On the other hand, the relative width of *t-Rec* can be also above one, and it is positively correlated to the incoherence of the base forecasts.

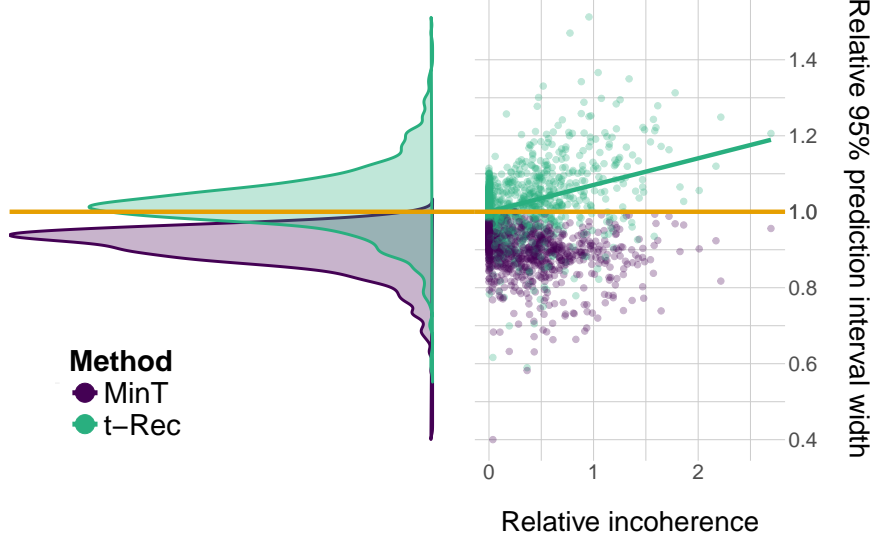


Figure 3: Left: distribution of the relative widths, i.e., reconciled PI width/base forecast PI width. We consider the 95% prediction intervals for the upper series for *MinT* (purple) and *t-Rec* (green), across 1000 simulations. While *MinT* always narrows the prediction intervals, *t-Rec* either widens or narrows them. Right: for each simulation, the relative widths of *MinT* and *t-Rec* are plotted against the incoherence $|\widehat{\mathbf{Ab}} - \widehat{u}|$, normalized by the standard deviation of the base forecasts (relative incoherence). Notably, *t-Rec* exhibits correlation, with interval widths expanding as incoherence grows.

In Table 1, we report the geometric mean, over the simulations, of the relative width of the prediction intervals for *MinT* and *t-Rec*, for 80% and 95% intervals. For *MinT*, the relative width is less or equal to 1 and remains constant across confidence levels, as it only depends on the ratio of the standard deviations of the reconciled and the base forecasts. In contrast, the relative width of *t-Rec* varies with the confidence level. Due to the heavier tails of the t-distribution compared to the Gaussian, *t-Rec* has higher relative width at the 95% level than at the 80%.

Relative width of the prediction intervals				
	80%		95%	
	<i>MinT</i>	<i>t-Rec</i>	<i>MinT</i>	<i>t-Rec</i>
U	0.90	0.99	0.90	1.02
B1	0.95	1.01	0.95	1.05
B2	0.95	1.01	0.95	1.05

Table 1: Geometric average over 1000 experiments of the relative width of 80% and 95% prediction intervals. A value smaller than 1 implies that on average reconciliation shortens the prediction intervals.

In Fig. 4, we compare the *MinT* and *t-Rec* forecast distributions of the upper-level series for two different simulation runs. We also include the densities of the base forecast distribution and the bottom-up distribution, defined as $\widehat{\pi}_{BU} = MVN(\widehat{\mathbf{Ab}}, \widehat{\mathbf{A}}\widehat{\Sigma}_B\mathbf{A}^T)$. When the incoherence $|\widehat{\mathbf{Ab}} - \widehat{u}|$ is low (left panel), the reconciled distributions of *MinT* and *t-Rec* are nearly identical. In contrast, when the incoherence is large (right panel), the distribution of *t-Rec* has heavier tails than that of *MinT*.

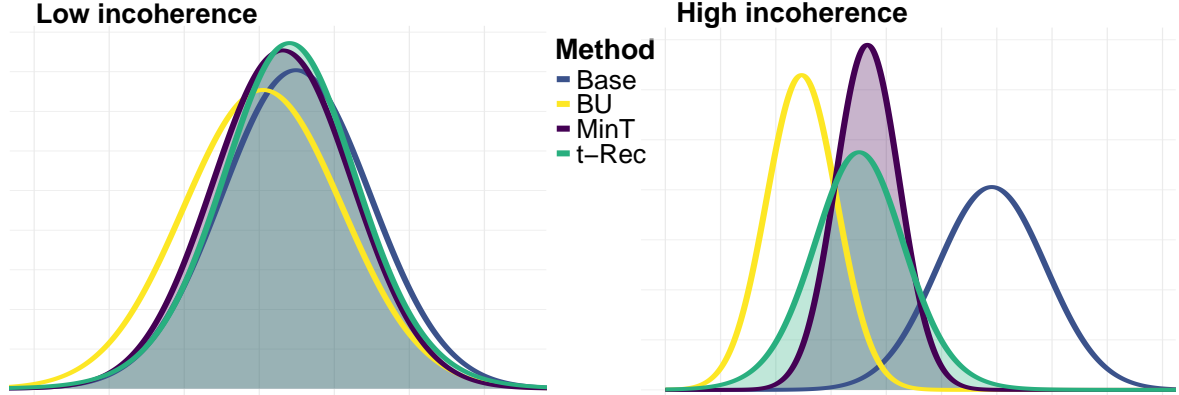


Figure 4: Comparison of the predictive densities for the upper time series of the minimal hierarchy. *Base* is the upper base forecast, *BU* is the bottom-up distribution for the upper obtained by summing the base bottom forecasts. Left: a simulation with little incoherence, where the densities mostly overlap. Right: a simulation with large incoherence, where *t-Rec* has heavier tails than *MinT*.

5. Experiments on real datasets

We evaluate the performance of *t-Rec* and *MinT* on three real-world datasets. The first is a novel dataset that we introduce and refer to as *Swiss tourism*, while the other two are established Australian tourism datasets commonly used in the literature.

The code related to the proposed method and the Swiss tourism dataset is available for reviewers on an anonymous GitHub¹. Upon acceptance, we plan to release our software, including the Swiss tourism dataset, in a package.

Swiss tourism. Switzerland is divided in 26 administrative regions, called cantons, listed in Table 2.

Abbr.	Canton	Abbr.	Canton	Abbr.	Canton
AG	Aargau	NW	Nidwalden	AI	Appenzell Innerrhoden
OW	Obwalden	AR	Appenzell Ausserrhoden	SG	St. Gallen
BE	Bern	SH	Schaffhausen	SO	Solothurn
BL	Basel-Landschaft	BS	Basel-Stadt	FR	Fribourg
GE	Geneva	GL	Glarus	GR	Graubünden
JU	Jura	LU	Lucerne	NE	Neuchâtel
SZ	Schwyz	TG	Thurgau	TI	Ticino
UR	Uri	VD	Vaud	VS	Valais
ZG	Zug	ZH	Zurich		

Table 2: List of the 26 Swiss cantons.

We collected monthly records of overnight stays from the Swiss Federal Statistical Office website². The data are originally disaggregated by both canton and country of origin of the tourists. However, for our analysis, we focus solely on the disaggregation by canton. This choice avoids issues with intermittency and sparsity, which occur in more disaggregated series and would invalidate the assumption of Gaussianity of the residuals used in our model.

The resulting hierarchy consists of 26 bottom-level series (one for each canton) and one top-level series (national total). The data comprises 241 monthly observations, from January 2005 to January 2025.

¹Link to Anonymized GitHub

²<https://www.pxweb.bfs.admin.ch/pxweb/en/>

Australian tourism. The other two datasets (*Australian Tourism-M* and *Australian Tourism-Q*) refer to Australian domestic overnight trips ³.

Australian Tourism-M dataset is derived from the file *TourismData_v3.csv*, available on Rob J Hyndman's website ⁴. It consists of monthly time series structured into a three-level hierarchy. The bottom level includes 76 series representing Australian regions, which are then aggregated into 27 zones, 7 states, and the total. This dataset spans from January 1998 to December 2016, covering 228 time points. For a detailed breakdown of this geographical hierarchy, we refer to Table 6 in Wickramasuriya et al. (2019).

We obtain *Australian Tourism-Q* from the **tsibble** R package (Wang, Cook & Hyndman, 2020). It contains quarterly data; it follows a two-level hierarchy, similar to the previous dataset but without the zone level. This dataset covers 20 years, from January 1998 to December 2017, for a total of 80 observations. The main features of all datasets are summarized in Table 3.

Dataset	Frequency	Levels	n_b	n_u	n	Length
Swiss Tourism	Monthly	1	26	1	27	240
Australian Tourism-M	Monthly	3	76	35	111	228
Australian Tourism-Q	Quarterly	2	76	8	84	80

Table 3: Summary of the datasets used in the paper.

Experimental setting. We compute the base forecasts for each time series using the ets model from the **forecast** R package Hyndman & Khandakar (2008). We only consider ets models with additive noise since our model assumes the predictive distribution of the base forecasts to be Gaussian. We compare the base forecasts with the forecast reconciled by *t-Rec* and *MinT*.

We consider different training lengths; for each training length, we perform repeated experiments with a rolling origin. We use 100 rolling origins for the monthly dataset. With *Australian Tourism-Q*, which has less observation, we use as many rolling origins as possible, depending on the training length.

Evaluation metrics. We assess the point forecasts through the Mean Squared Error (MSE), averaged over the rolling origins:

$$MSE = \frac{1}{R} \sum_{i=1}^R \|\tilde{\mathbf{y}}_i - \mathbf{y}_i\|_2^2,$$

where $\|\cdot\|_2$ is the Euclidean distance, R is the number of rolling origins, $\tilde{\mathbf{y}}_i \in \mathbb{R}^n$ is the vector of the point forecasts for the i -th rolling origin, and $\mathbf{y}_i \in \mathbb{R}^n$ is the vector of the corresponding actual values. We eventually report the relative MSE, i.e., the ratio between the MSE of the reconciled and the base forecasts:

$$RelMSE = \frac{MSE}{MSE_{base}}. \quad (16)$$

For each series j , with $j = 1, \dots, n$, we assess the predictive distribution using the Continuous Ranked Probability Score (CRPS) (Gneiting & Raftery, 2007):

$$CRPS_j = \frac{1}{R} \sum_{i=1}^R \int_{-\infty}^{+\infty} (F_{i,j}(x) - \mathbb{I}(x \geq y_{i,j}))^2 dx$$

where $F_{i,j}$ is the predictive CDF for the i -th rolling origin and series j and $y_{i,j}$ is the corresponding actual value. We compute the CRPS for both the Gaussian and t distributions in closed form using the **scoringRules** R package (Jordan, Krüger & Lerch, 2019). For each series, we score the prediction intervals using the Mean Interval Score (MIS) (Gneiting & Raftery, 2007):

$$MIS_j = \frac{1}{R} \sum_{i=1}^R \left((u_{i,j}^\alpha - l_{i,j}^\alpha) + \frac{2}{\alpha} [(l_{i,j}^\alpha - y_{i,j})\mathbb{I}(y_{i,j} < l_{i,j}^\alpha) + (y_{i,j} - u_{i,j}^\alpha)\mathbb{I}(y_{i,j} > u_{i,j}^\alpha)] \right)$$

³<https://www.tra.gov.au/>

⁴<https://robjhyndman.com/data/>

where $l_{i,j}^\alpha$ and $u_{i,j}^\alpha$ are the lower and upper bounds of the α -level prediction interval for the i -th rolling origin and series j , and $y_{i,j}$ is the corresponding actual value. We consider the 80% and 95% prediction intervals. The CRPS and MIS are univariate scale-dependent scoring rules; we follow the approach of Girolimetto et al. (2024) to aggregate the n scores into a single value by computing the geometric mean of the relative scores with respect to the base forecasts:

$$RelCRPS = \left(\prod_{j=1}^n \frac{CRPS_j}{CRPS_{j,base}} \right)^{\frac{1}{n}}, \quad (17)$$

and we do the same with the relative MIS scores for the 80% and 95% prediction intervals.

Finally, we apply the non-parametric Friedman test with Nemenyi post hoc test to check the significance of the differences, using the `tsutils` R package (Kourentzes, 2023).

5.1. Swiss Tourism results

We consider training lengths from 30 (two and a half years) to 60 (five years); the results are shown in Fig. 5 as a function of the training length.

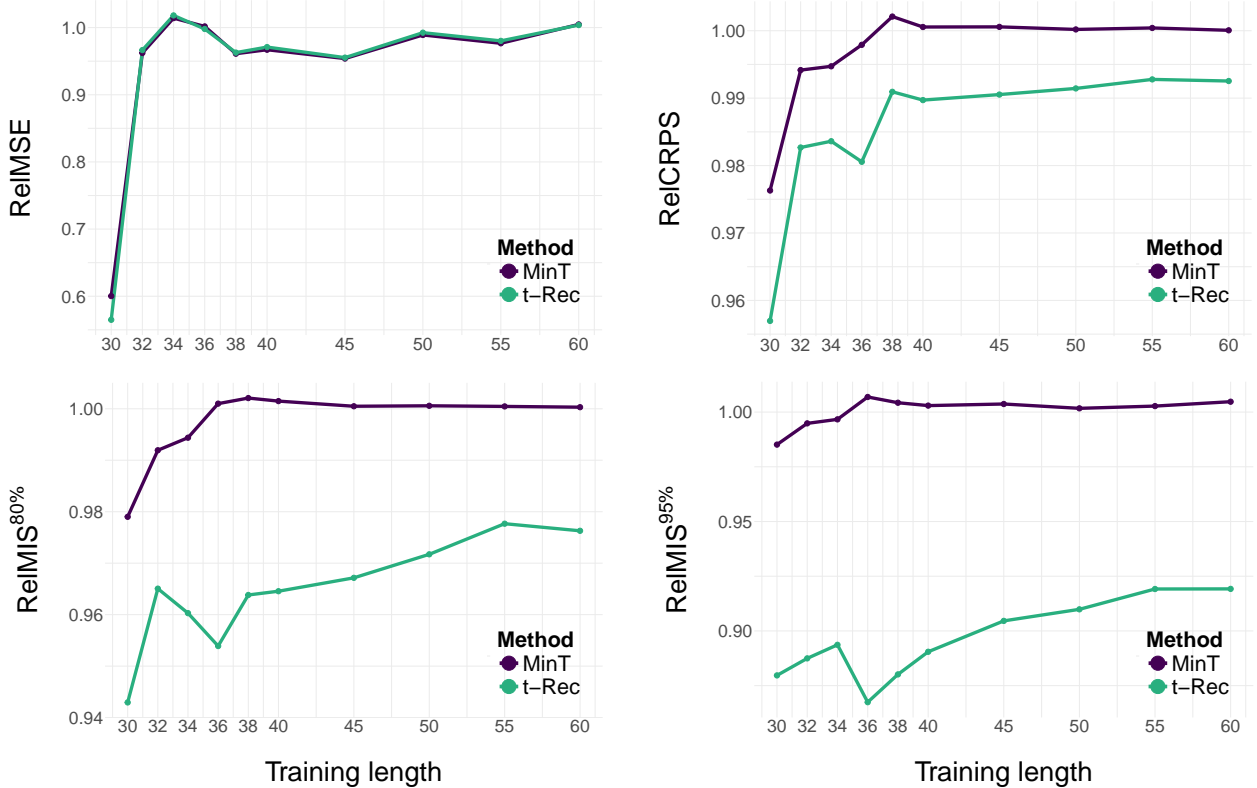


Figure 5: Results on the *Swiss Tourism* dataset for *MinT* (purple) and *t-Rec* (green), for the relative MSE (top-left), CRPS (top-right), and MIS (bottom-left: 80%, bottom-right: 95%). A relative score lower than 1 means improvement over the base forecasts.

On the MSE, *t-Rec* and *MinT* perform similarly across all training lengths (top-left plot). However, *t-Rec* shows a clear improvement in the predictive distribution, with relative CRPS (top-right) and MIS (bottom) consistently below *MinT*. Since the CRPS averages the quantile loss across all quantiles (Hyndman & Athanasopoulos, 2021, Chap. 5.9) and *t-Rec* particularly enhances the tails of the predictive distributions, the improvement is more pronounced for the MIS, especially for the 95% intervals. Indeed, the t-distribution has polynomial tails, which allocate more probability mass to the extremes compared to the exponential tails of the Gaussian distribution used by *MinT*. Moreover, *t-Rec* provides better coverage than *MinT* (Fig. 6).

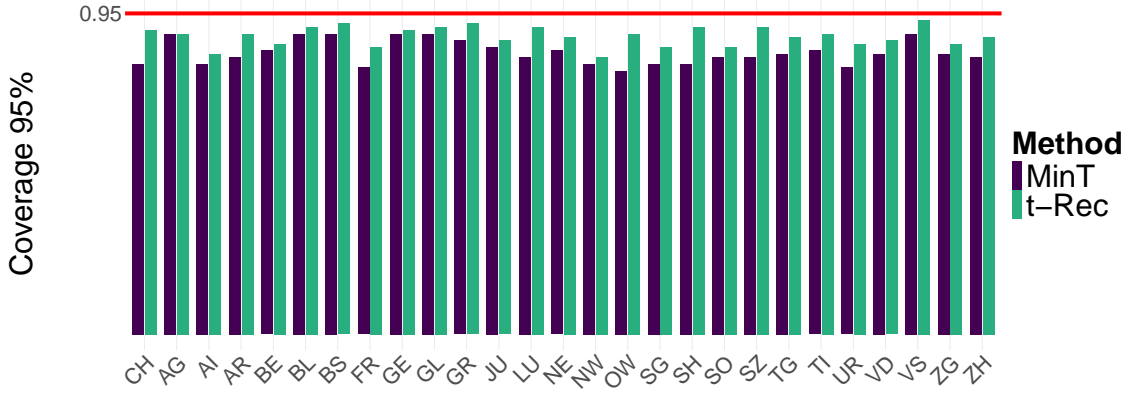


Figure 6: Coverage of the 95% prediction intervals across 100 rolling origins (training length = 40). For each series, *t-Rec* achieves coverage closer to the target (red line) than *MinT*.

Fig. 7 reports the results of the Friedman test for a training length of 40 observations. This non-parametric test assesses whether the differences in model rankings are statistically significant. To identify which specific models differ significantly, a Nemenyi post-hoc test was applied.

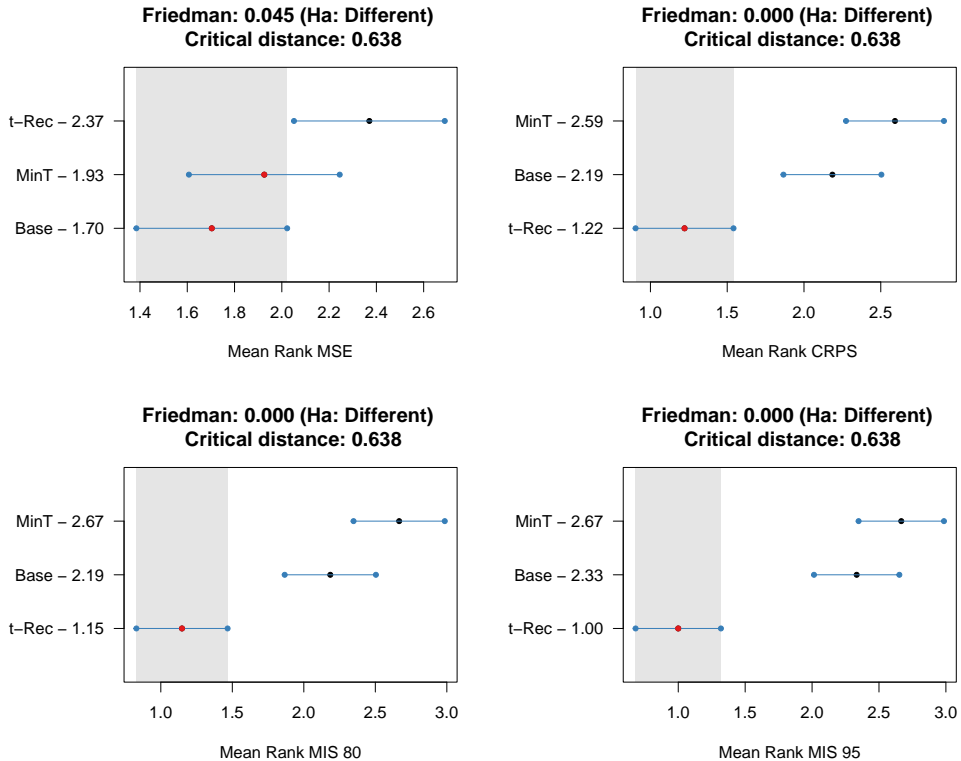


Figure 7: Friedman and post-hoc Nemenyi tests results for training length of 40 in the *Swiss Tourism* dataset for the MSE (top-left), CRPS (top-right), and MIS (bottom-left: 80%, bottom-right: 95%).

Fig. 8 reports the relative MIS for the 95% prediction intervals at the canton level for a training length of 40 observations. These results further confirm that *t-Rec* yields higher-scoring prediction intervals than *MinT*. Moreover, Fig. 9 shows how the 95% prediction interval width, both for the upper-level series (left panel) and the geometric mean across bottom-level series (right panel), varies with the incoherence. There is a clear

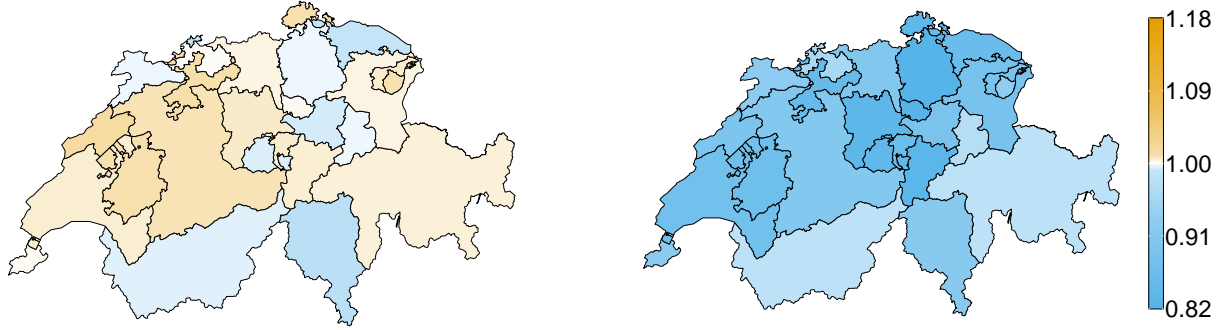


Figure 8: Relative MIS^{95%} of *MinT* (left) and *t-Rec* (right) for each canton of the *Swiss Tourism* dataset (training length 40). Orange-colored cantons indicate worse performance compared to the base forecasts (ratio > 1). *t-Rec* consistently improves MIS^{95%} across all cantons and achieves greater absolute gains compared to *MinT*.

correlation between the interval widths of *t-Rec* and the amount of incoherence. In contrast, *MinT* shows no such dependence.

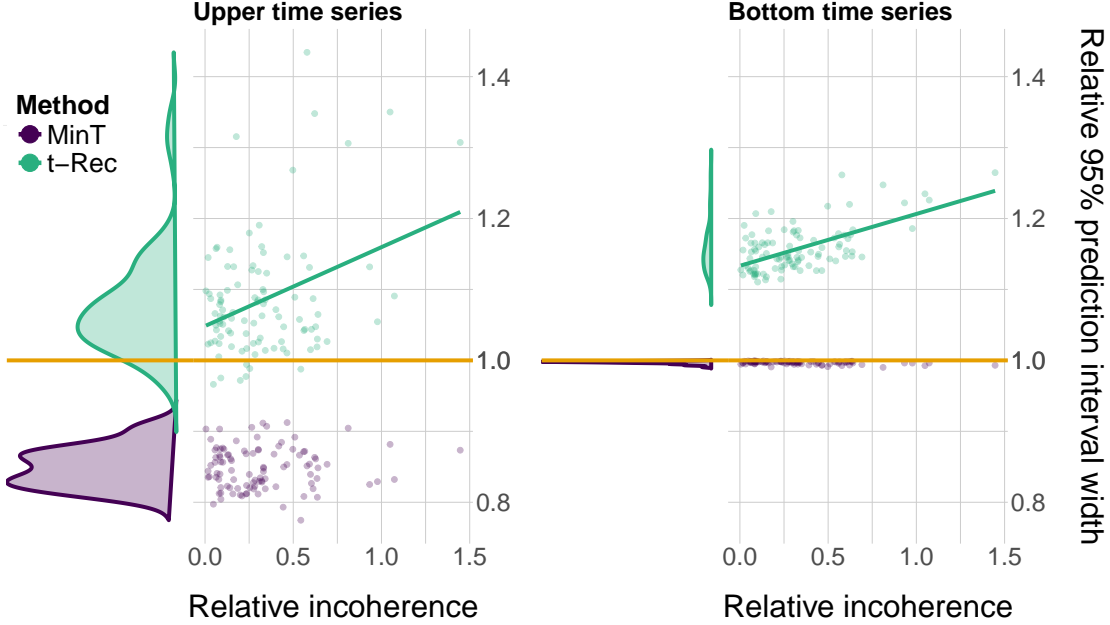


Figure 9: Relative widths, i.e., reconciled PI width/base forecast PI width, of the 95% prediction intervals. In the left panel we show the relative width of the upper series; in the right panel we show the geometric mean of the relative widths of the bottom series. For each rolling origin, we plot the relative widths of *MinT* (purple) and *t-Rec* (green) against the relative incoherence $|\hat{\mathbf{Ab}} - \hat{u}|$, normalized by the standard deviation of the base forecasts. *t-Rec* exhibits a positive correlation, with interval widths expanding as incoherence grows. In contrast, *MinT* maintains narrower intervals regardless of incoherence.

5.2. Australian Tourism results

On both the *Australian tourism-M* and *Australian tourism-Q* datasets, we observe patterns consistent with those found in the *Swiss Tourism* dataset. In terms of MSE, *t-Rec* and *MinT* perform similarly, indicating comparable point forecast accuracy. However, *t-Rec* yields better probabilistic forecasts, with a slight advantage in CRPS and substantial improvements in MIS, particularly at the 95% level, reflecting more reliable prediction intervals (Fig. 10).

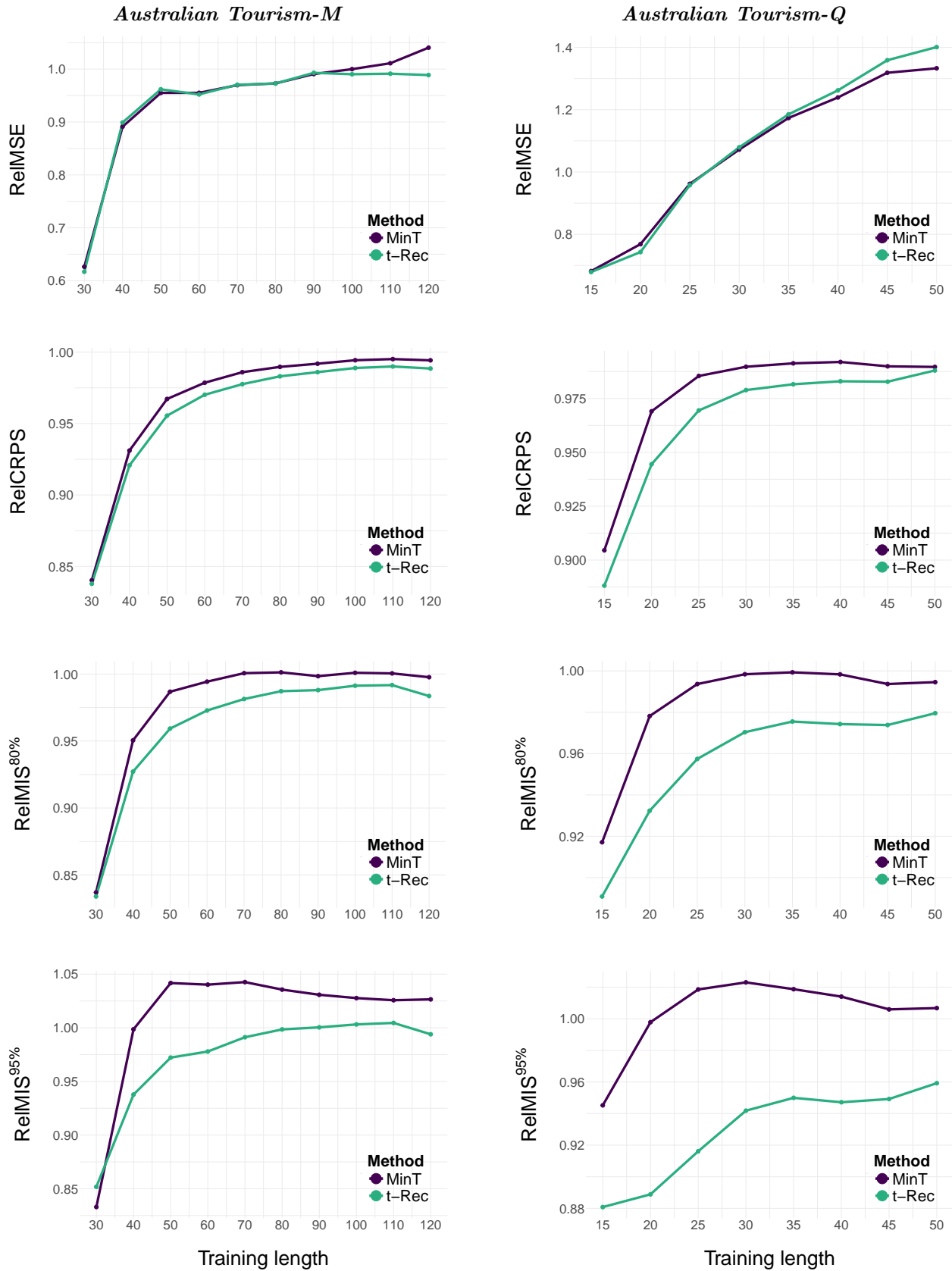


Figure 10: Results on the *Australian Tourism-M* (left column) and *Australian Tourism-Q* (right column) datasets for *MinT* (purple) and *t-Rec* (green). A relative score lower than 1 means improvement over the base forecasts.

We also compute the geometric mean of prediction interval widths and the arithmetic mean of coverage rates across the time series. We report the results for two different training lengths in Table 4. As for the *Swiss Tourism* dataset, *t-Rec* produces wider intervals than *MinT*, resulting in average coverage rates closer to the nominal levels (0.8 or 0.95).

		Australian Tourism - M				Australian Tourism - Q			
		Train 55		Train 110		Train 25		Train 40	
Level		<i>MinT</i>	<i>t-Rec</i>	<i>MinT</i>	<i>t-Rec</i>	<i>MinT</i>	<i>t-Rec</i>	<i>MinT</i>	<i>t-Rec</i>
PI Width	80%	0.87	0.92	0.91	0.94	0.95	1.09	0.96	1.12
	95%	0.87	0.93	0.91	0.94	0.95	1.11	0.96	1.13
Coverage	80%	0.73	0.76	0.78	0.80	0.69	0.76	0.69	0.77
	95%	0.88	0.90	0.91	0.92	0.86	0.92	0.87	0.93

Table 4: Prediction interval (PI) width and coverage at the 80% and 95% confidence levels for the *Australian Tourism-M* and *Australian Tourism-Q* datasets. Results are reported for various training lengths.

5.3. Comparison between diagonal and full Ψ_0

We now consider a variant of *t-Rec*, denoted *t-Rec-Diag*, in which the prior scale matrix Ψ_0 is specified in the same way as in *t-Rec*, but is restricted to be diagonal. We compare the performance of *t-Rec*, *t-Rec-Diag*, and *MinT* on *Swiss tourism* in Fig. 11 and on *Australian Tourism-M* and *Australian Tourism-Q* in Fig. D.14 of Appendix D.

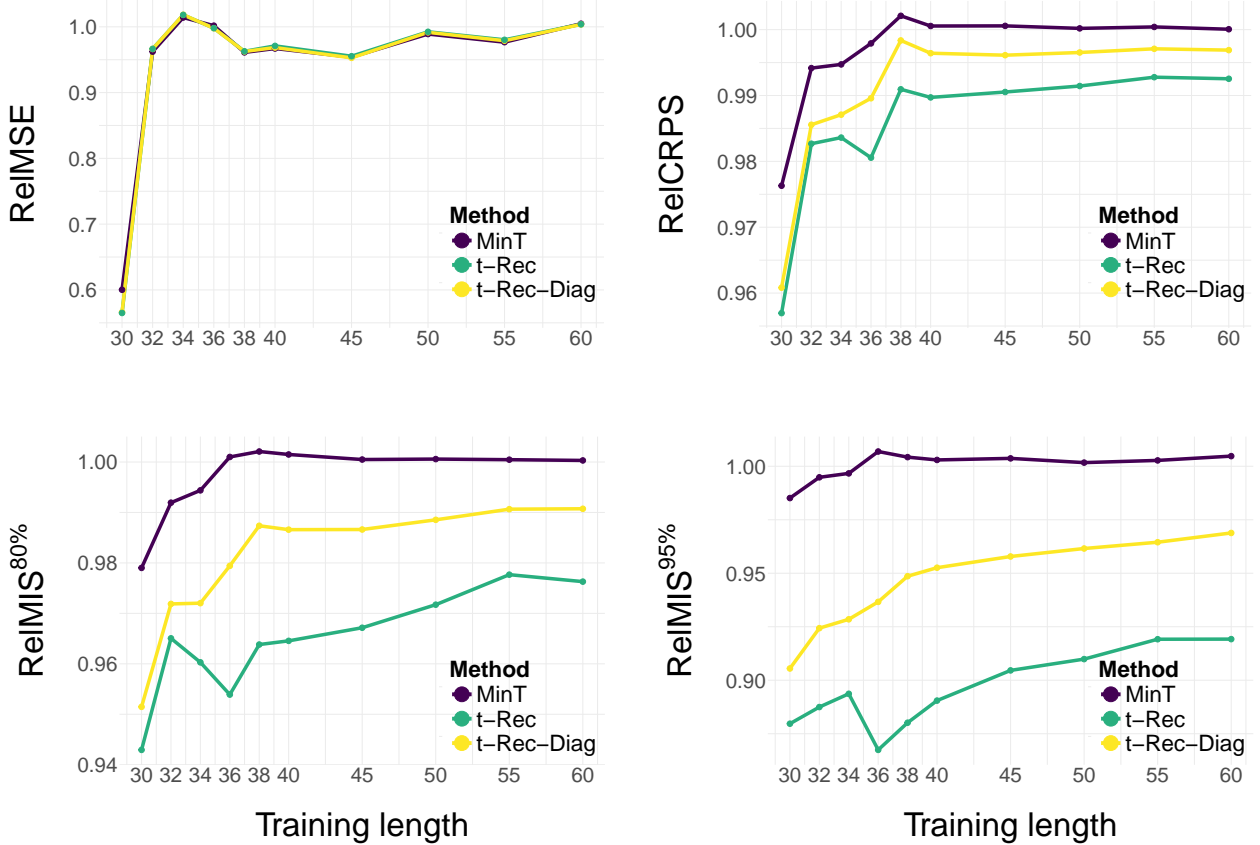


Figure 11: Results on *Swiss Tourism* dataset for *MinT* (purple), *t-Rec* (green) and *t-Rec-Diag* (yellow). A relative score lower than 1 means improvement over the base forecasts.

Overall, we can draw some common conclusions. On the point forecasts, *MinT*, *t-Rec* and *t-Rec-Diag* achieve a practically equivalent performance. However, differences emerge in the probabilistic scores. For both CRPS and MIS across various confidence levels, *t-Rec-Diag* outperforms *MinT*, highlighting the benefit of modeling uncertainty in \mathbf{W} . Furthermore, the superiority of *t-Rec* over *t-Rec-Diag* indicates that the prior information on the correlations among residuals from naive and seasonal naive methods is informative and contributes to improved predictive performance. Overall, *t-Rec* is the reconciliation method we recommend.

6. Conclusion

We propose *t-Rec*, a Bayesian method for probabilistic reconciliation that accounts for the uncertainty on the covariance matrix. We obtain in closed-form a multivariate-t reconciled predictive distribution. Empirical results show that *t-Rec* consistently outperforms *MinT* on the prediction intervals, while maintaining comparable point forecast accuracy. These gains persist even when the number of observations is small relative to the number of series, and are robust across different training lengths. Overall, our findings underscore the importance of modeling covariance matrix uncertainty to enhance the quality of probabilistic forecasts. Our analysis focuses on the cross-sectional hierarchical setting; we leave for future studies the extension to temporal hierarchies. Finally, we acknowledge the limitations of the IW prior, particularly in high-dimensional settings (Gelman, 2006). Future work will explore more flexible priors for the covariance matrix and assess their impact on reconciliation performance.

References

Carrara, C., Zambon, L., Azzimonti, D., & Corani, G. (2025). A novel shrinkage estimator of the covariance matrix for hierarchical time series. In E. di Bella, V. Gioia, C. Lagazio, & S. Zaccarin (Eds.), *Statistics for Innovation I* (pp. 140–145). Cham: Springer Nature Switzerland.

Corani, G., Azzimonti, D., Augusto, J. P., & Zaffalon, M. (2020). Probabilistic Reconciliation of Hierarchical Forecast via Bayes' Rule. In *Proc. European Conf. On Machine Learning and Knowledge Discovery in Database ECML/PKDD* (pp. 211–226). volume 3.

Di Fonzo, T., & Girolimetto, D. (2024). Forecast combination-based forecast reconciliation: Insights and extensions. *International Journal of Forecasting*, 40, 490–514.

Gelman, A. (2006). Prior distributions for variance parameters in hierarchical models (Comment on Article by Browne and Draper). *Bayesian Analysis*, 1, 515–534.

Gelman, A., Carlin, J., Stern, H., Dunson, D., Vehtari, A., & Rubin, D. (2013). *Bayesian Data Analysis (3rd ed.)*. Chapman and Hall/CRC.

Girolimetto, D., Athanasopoulos, G., Di Fonzo, T., & Hyndman, R. J. (2024). Cross-temporal probabilistic forecast reconciliation: Methodological and practical issues. *International Journal of Forecasting*, 40, 1134–1151.

Girolimetto, D., & Di Fonzo, T. (2024). Point and probabilistic forecast reconciliation for general linearly constrained multiple time series. *Statistical Methods & Applications*, 33, 581–607.

Gneiting, T., & Raftery, A. E. (2007). Strictly proper scoring rules, prediction, and estimation. *Journal of the American statistical Association*, 102, 359–378.

Gupta, A. K., & Nagar, D. K. (2018). *Matrix variate distributions*. Chapman and Hall/CRC.

Hollyman, R., Petropoulos, F., & Tipping, M. E. (2021). Understanding forecast reconciliation. *European Journal of Operational Research*, 294, 149–160.

Hyndman, R. J., & Athanasopoulos, G. (2021). *Forecasting: principles and practice, 3rd edition*. OTexts. URL: [OTexts.com/fpp3](https://otexts.com/fpp3).

Hyndman, R. J., & Khandakar, Y. (2008). Automatic time series forecasting: the forecast package for R. *Journal of statistical software*, 27, 1–22.

Johnson, S. G. (2008). *The NLOpt nonlinear-optimization package*. URL: <https://github.com/stevengj/nlopt>.

Jordan, A., Krüger, F., & Lerch, S. (2019). Evaluating Probabilistic Forecasts with scoringRules. *Journal of Statistical Software*, 90, 1–37.

Kotz, S., & Nadarajah, S. (2004). *Multivariate t-distributions and their applications*. Cambridge University Press.

Kourentzes, N. (2023). *tsutils: Time Series Exploration, Modelling and Forecasting*. R package version 0.9.4.

Panagiotelis, A., Athanasopoulos, G., Gamakumara, P., & Hyndman, R. J. (2021). Forecast reconciliation: A geometric view with new insights on bias correction. *International Journal of Forecasting*, 37, 343–359.

Panagiotelis, A., Gamakumara, P., Athanasopoulos, G., & Hyndman, R. J. (2023). Probabilistic forecast reconciliation: Properties, evaluation and score optimisation. *European Journal of Operational Research*, 306, 693–706.

Pritularga, K. F., Svetunkov, I., & Kourentzes, N. (2021). Stochastic coherency in forecast reconciliation. *International Journal of Production Economics*, 240, 108221.

Schäfer, J., & Strimmer, K. (2005). A shrinkage approach to large-scale covariance matrix estimation and implications for functional genomics. *Statistical applications in genetics and molecular biology*, 4.

Sherman, J., & Morrison, W. J. (1950). Adjustment of an inverse matrix corresponding to a change in one element of a given matrix. *The Annals of Mathematical Statistics*, 21, 124–127.

Svetunkov, I. (2023). *Forecasting and analytics with the augmented dynamic adaptive model (ADAM)*. CRC Press.

Vehtari, A., Gelman, A., & Gabry, J. (2017). Practical Bayesian model evaluation using leave-one-out cross-validation and WAIC. *Statistics and computing*, 27, 1413–1432.

Wang, E., Cook, D., & Hyndman, R. J. (2020). A new tidy data structure to support exploration and modeling of temporal data. *Journal of Computational and graphical Statistics*, 29, 466–478.

Wickramasuriya, S. L. (2017). *Optimal Forecasts for Hierarchical and Grouped Time Series*. Ph.D. thesis Monash University.

Wickramasuriya, S. L. (2024). Probabilistic forecast reconciliation under the Gaussian framework. *Journal of Business & Economic Statistics*, 42, 272–285.

Wickramasuriya, S. L., Athanasopoulos, G., & Hyndman, R. J. (2019). Optimal forecast reconciliation for hierarchical and grouped time series through trace minimization. *Journal of the American Statistical Association*, 114, 804–819.

Yang, Y. F., Athanasopoulos, G., Hyndman, R. J., & Panagiotelis, A. (2024). Forecast Linear Augmented Projection (FLAP): A free lunch to reduce forecast error variance. *arXiv preprint arXiv:2407.01868*, .

Zambon, L., Agosto, A., Giudici, P., & Corani, G. (2024a). Properties of the reconciled distributions for Gaussian and count forecasts. *International Journal of Forecasting*, 40, 1438–1448.

Zambon, L., Azzimonti, D., & Corani, G. (2024b). Efficient probabilistic reconciliation of forecasts for real-valued and count time series. *Statistics and Computing*, 34, 21.

Zambon, L., Azzimonti, D., Rubattu, N., & Corani, G. (2024c). Probabilistic reconciliation of mixed-type hierarchical time series. In *The 40th Conference on Uncertainty in Artificial Intelligence*.

Appendix A. Reconciliation via conditioning of multivariate t

Similarly to the Gaussian case (Zambon et al., 2024a), if the joint base forecast distribution is a multivariate t, then the reconciled distribution and the parameters can be computed in closed-form. Theorem 1 is proved by applying the following result to Eq. (7) with $\widehat{\Psi} = \frac{1}{\nu' - n + 1} \Psi'$ and $\widehat{\nu} = \nu' - n + 1$.

Proposition 1. *Let $\mathbf{A} \in \mathbb{R}^{(n-n_b) \times n_b}$ be the aggregation matrix of a hierarchy with n time series, and let the joint forecast distribution be a multivariate t: $\widehat{\mathbf{Y}} \sim \text{mt}(\widehat{\mathbf{y}}, \widehat{\Psi}, \widehat{\nu})$. Then, the reconciled distribution via conditioning of the n_b bottom series is still a multivariate t:*

$$\widetilde{\mathbf{B}} \sim \text{mt}(\widetilde{\mathbf{b}}, \widetilde{\Sigma}_B, \widetilde{\nu}), \quad (\text{A.1})$$

where

$$\widetilde{\mathbf{b}} = \widehat{\mathbf{b}} + \left(\widehat{\Psi}_{UB}^T - \widehat{\Psi}_B \mathbf{A}^T \right) \mathbf{Q}^{-1} (\mathbf{A} \widehat{\mathbf{b}} - \widehat{\mathbf{u}}), \quad (\text{A.2})$$

$$\widetilde{\Sigma}_B = C \left[\widehat{\Psi}_B - \left(\widehat{\Psi}_{UB}^T - \widehat{\Psi}_B \mathbf{A}^T \right) \mathbf{Q}^{-1} \left(\widehat{\Psi}_{UB}^T - \widehat{\Psi}_B \mathbf{A}^T \right)^T \right], \quad (\text{A.3})$$

$$\widetilde{\nu} = \widehat{\nu} + n - n_b, \quad (\text{A.4})$$

and

$$C = \frac{\widehat{\nu} + (\mathbf{A} \widehat{\mathbf{b}} - \widehat{\mathbf{u}})^T \mathbf{Q}^{-1} (\mathbf{A} \widehat{\mathbf{b}} - \widehat{\mathbf{u}})}{\widehat{\nu} + (n - n_b)},$$

$$\mathbf{Q} = \widehat{\Psi}_U - \widehat{\Psi}_{UB} \mathbf{A}^T - \mathbf{A} \widehat{\Psi}_{UB}^T + \mathbf{A} \widehat{\Psi}_B \mathbf{A}^T. \quad (\text{A.5})$$

To prove Proposition 1, we first state two technical lemmas about key properties of the multivariate t distribution. For a proof of these lemmas, we refer to Kotz & Nadarajah (2004).

Lemma 1. *Let \mathbf{X} be a n -dimensional random vector distributed as a multivariate t:*

$$\mathbf{X} \sim \text{mt}(\boldsymbol{\mu}, \boldsymbol{\Sigma}, \nu),$$

and let $\mathbf{V} \in \mathbb{R}^{n \times n}$ be full-rank. Then, the random vector $\mathbf{V}\mathbf{X}$ is distributed as a multivariate t:

$$\mathbf{V}\mathbf{X} \sim \text{mt}(\mathbf{V}\boldsymbol{\mu}, \mathbf{V}\boldsymbol{\Sigma}\mathbf{V}^T, \nu).$$

Lemma 2. *Let $\mathbf{X} = \begin{bmatrix} \mathbf{X}_1 \\ \mathbf{X}_2 \end{bmatrix} \sim \text{mt} \left(\begin{bmatrix} \boldsymbol{\mu}_1 \\ \boldsymbol{\mu}_2 \end{bmatrix}, \begin{bmatrix} \boldsymbol{\Sigma}_{11} & \boldsymbol{\Sigma}_{12} \\ \boldsymbol{\Sigma}_{21} & \boldsymbol{\Sigma}_{22} \end{bmatrix}, \nu \right)$, where $\mathbf{X} \in \mathbb{R}^n$, $\mathbf{X}_1 \in \mathbb{R}^{n_1}$, $\mathbf{X}_2 \in \mathbb{R}^{n_2}$ and $n_1 + n_2 = n$. Then, the conditional distribution of \mathbf{X}_1 given \mathbf{X}_2 is still a multivariate t:*

$$\mathbf{X}_1 | \mathbf{X}_2 \sim \text{mt}(\boldsymbol{\mu}_{1|2}, \boldsymbol{\Sigma}_{1|2}, \nu_{1|2}), \quad (\text{A.6})$$

where

$$\boldsymbol{\mu}_{1|2} = \boldsymbol{\mu}_1 + \boldsymbol{\Sigma}_{12} \boldsymbol{\Sigma}_{22}^{-1} (\mathbf{x}_2 - \boldsymbol{\mu}_2), \quad (\text{A.7})$$

$$\boldsymbol{\Sigma}_{1|2} = \frac{\nu + (\mathbf{x}_2 - \boldsymbol{\mu}_2)^T \boldsymbol{\Sigma}_{22}^{-1} (\mathbf{x}_2 - \boldsymbol{\mu}_2)}{\nu + n_2} [\boldsymbol{\Sigma}_{11} - \boldsymbol{\Sigma}_{12} \boldsymbol{\Sigma}_{22}^{-1} \boldsymbol{\Sigma}_{21}], \quad (\text{A.8})$$

$$\nu_{1|2} = \nu + n_2. \quad (\text{A.9})$$

Proof of Proposition 1. Let us define $\mathbf{T} \in \mathbb{R}^{n \times n}$ as

$$\mathbf{T} = \begin{bmatrix} \mathbf{0} & \mathbf{I}_{n_b} \\ \mathbf{I}_{n-n_b} & -\mathbf{A} \end{bmatrix},$$

and let $\mathbf{Z} := \mathbf{T}\widehat{\mathbf{Y}}$. Since \mathbf{T} is full-rank, from Lemma 1, \mathbf{Z} is a multivariate t:

$$\mathbf{Z} \sim \text{mt}(\mathbf{T}\widehat{\mathbf{y}}, \mathbf{T}\widehat{\Psi}\mathbf{T}^T, \widehat{\nu}), \quad (\text{A.10})$$

where

$$\begin{aligned}\mathbf{T}\hat{\mathbf{y}} &= \begin{bmatrix} \hat{\mathbf{b}} \\ \hat{\mathbf{u}} - \mathbf{A}\hat{\mathbf{b}} \end{bmatrix}, \\ \mathbf{T}\hat{\Psi}\mathbf{T}^T &= \begin{bmatrix} \hat{\Psi}_B & \hat{\Psi}_{UB}^T - \hat{\Psi}_B\mathbf{A}^T \\ \hat{\Psi}_{UB} - \mathbf{A}\hat{\Psi}_B & \mathbf{Q} \end{bmatrix},\end{aligned}\tag{A.11}$$

and $\mathbf{Q} = \hat{\Psi}_U - \hat{\Psi}_{UB}\mathbf{A}^T - \mathbf{A}\hat{\Psi}_{UB}^T + \mathbf{A}\hat{\Psi}_B\mathbf{A}^T$. Since

$$\mathbf{Z} = \begin{bmatrix} \hat{\mathbf{B}} \\ \hat{\mathbf{U}} - \mathbf{A}\hat{\mathbf{B}} \end{bmatrix} =: \begin{bmatrix} \mathbf{Z}_1 \\ \mathbf{Z}_2 \end{bmatrix},$$

the reconciled bottom distribution is given by the conditional distribution of \mathbf{Z}_1 given $\mathbf{Z}_2 = 0$. From Lemma 2, we have that

$$\mathbf{Z}_1 | \mathbf{Z}_2 = 0 \sim \text{mt}(\boldsymbol{\mu}_{1|2}, \boldsymbol{\Sigma}_{1|2}, \nu_{1|2}),$$

where

$$\begin{aligned}\boldsymbol{\mu}_{1|2} &= \hat{\mathbf{b}} + (\hat{\Psi}_{UB}^T - \hat{\Psi}_B\mathbf{A}^T)\mathbf{Q}^{-1}(\mathbf{A}\hat{\mathbf{b}} - \hat{\mathbf{u}}) = \tilde{\mathbf{b}}, \\ \nu_{1|2} &= \hat{\nu} + (n - n_b) = \tilde{\nu}, \\ \boldsymbol{\Sigma}_{1|2} &= \frac{\hat{\nu} + (\mathbf{A}\hat{\mathbf{b}} - \hat{\mathbf{u}})^T\mathbf{Q}^{-1}(\mathbf{A}\hat{\mathbf{b}} - \hat{\mathbf{u}})}{\hat{\nu} + (n - n_b)} \left[\hat{\Psi}_B - (\hat{\Psi}_{UB}^T - \hat{\Psi}_B\mathbf{A}^T)\mathbf{Q}^{-1}(\hat{\Psi}_{UB}^T - \hat{\Psi}_B\mathbf{A}^T)^T \right] \\ &= C \left[\hat{\Psi}_B - (\hat{\Psi}_{UB}^T - \hat{\Psi}_B\mathbf{A}^T)\mathbf{Q}^{-1}(\hat{\Psi}_{UB}^T - \hat{\Psi}_B\mathbf{A}^T)^T \right] = \tilde{\boldsymbol{\Sigma}}_B.\end{aligned}$$

□

Appendix B. Simulation setup

For the experiments in Sect. 4, we adopt a simulation framework similar to that described in Sect. 3.4 of Wickramasuriya et al. (2019). We consider the minimal hierarchy of Fig. 2. The length of the time series is set to 12. The bottom-level time series are simulated using a basic structural time series model defined as:

$$\mathbf{b}_t = \boldsymbol{\mu}_t + \boldsymbol{\gamma}_t + \boldsymbol{\eta}_t,$$

where $\boldsymbol{\mu}_t$ is the trend component, $\boldsymbol{\gamma}_t$ is the seasonal component, and $\boldsymbol{\eta}_t$ is the error component. The trend component evolves according to a local linear trend model:

$$\begin{aligned}\boldsymbol{\mu}_t &= \boldsymbol{\mu}_{t-1} + \boldsymbol{\nu}_t + \boldsymbol{\varepsilon}_t, & \boldsymbol{\varepsilon}_t &\sim \mathcal{N}(0, 2I_2), \\ \boldsymbol{\nu}_t &= \boldsymbol{\nu}_{t-1} + \boldsymbol{\zeta}_t, & \boldsymbol{\zeta}_t &\sim \mathcal{N}(0, 0.007I_2),\end{aligned}$$

where $\boldsymbol{\varepsilon}_t$, $\boldsymbol{\zeta}_t$, and $\boldsymbol{\omega}_t$ are mutually independent and also independent over time. The seasonal component is defined by:

$$\boldsymbol{\gamma}_t = - \sum_{i=1}^{s-1} \boldsymbol{\gamma}_{t-i} + \boldsymbol{\omega}_t, \quad \boldsymbol{\omega}_t \sim \mathcal{N}(0, 7I_2),$$

with the number of seasons per year set to $s = 4$ to reflect quarterly data. The initial states $\boldsymbol{\mu}_0$, $\boldsymbol{\nu}_0$, $\boldsymbol{\gamma}_0$, $\boldsymbol{\gamma}_1$, and $\boldsymbol{\gamma}_2$ are independently drawn from a multivariate normal distribution with mean zero and identity covariance matrix. The error component $\boldsymbol{\eta}_t$ for each series is generated from an ARIMA(1, 0, 1) model with $\phi_1 = 0.3$ and $\theta_1 = 0.5$; we use $\begin{bmatrix} 5 & 3 \\ 3 & 4 \end{bmatrix}$ as contemporaneous error covariance matrix, the same of series AA and AB in Wickramasuriya et al. (2019). Finally, the upper level series is obtained by summing the bottom-level series.

Appendix C. Significance results - Australian tourism

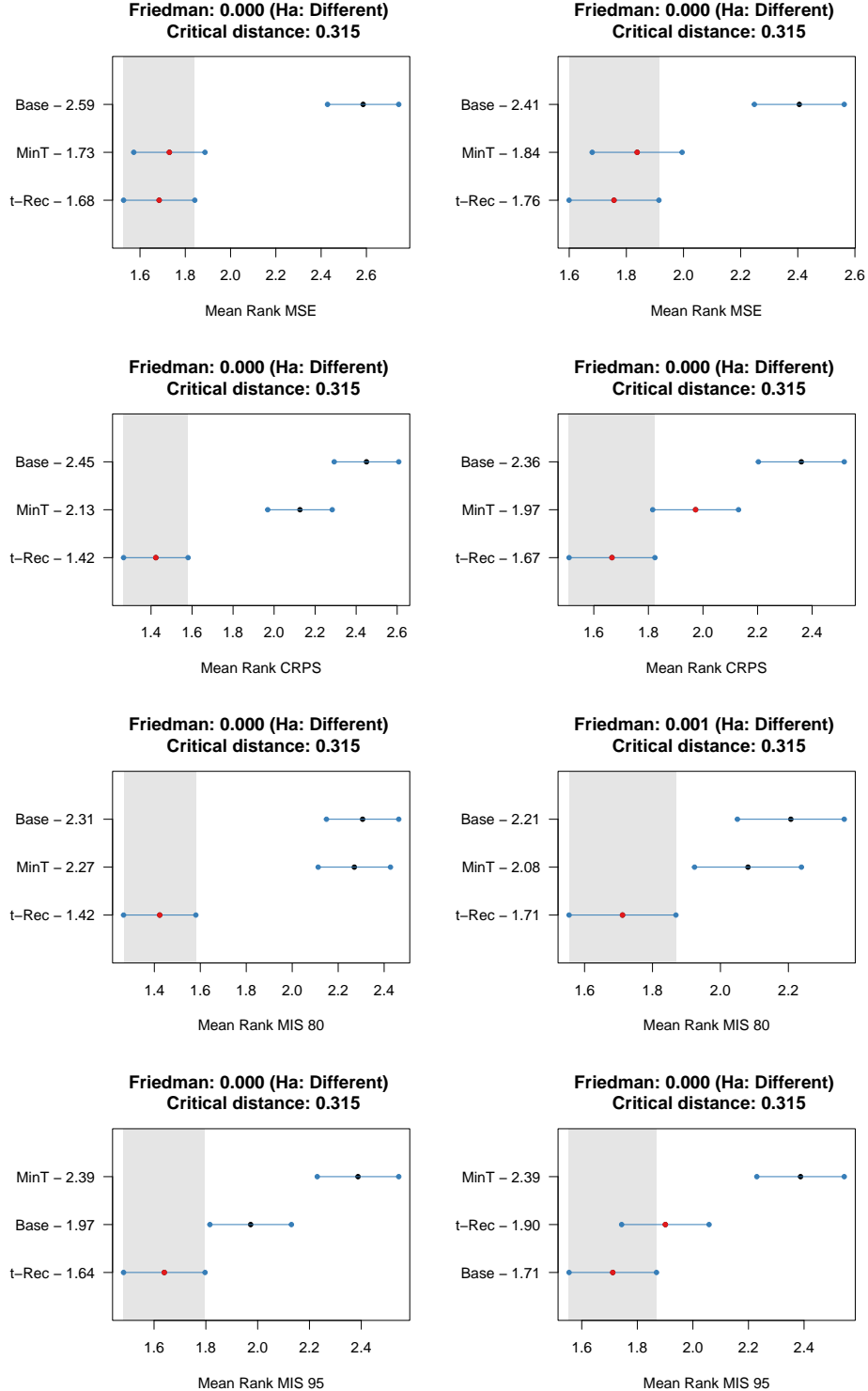


Figure C.12: Friedman and post-hoc Nemenyi tests results for the *Australian tourism-M* dataset. The columns represent different choices of training length: 55 and 110 observations, respectively. The rows correspond to the metrics: the first row shows the MSE, the second row displays the CRPS, the third row presents the MIS calculated for the 80% prediction interval, and the fourth the MIS calculated for the 95% prediction interval.

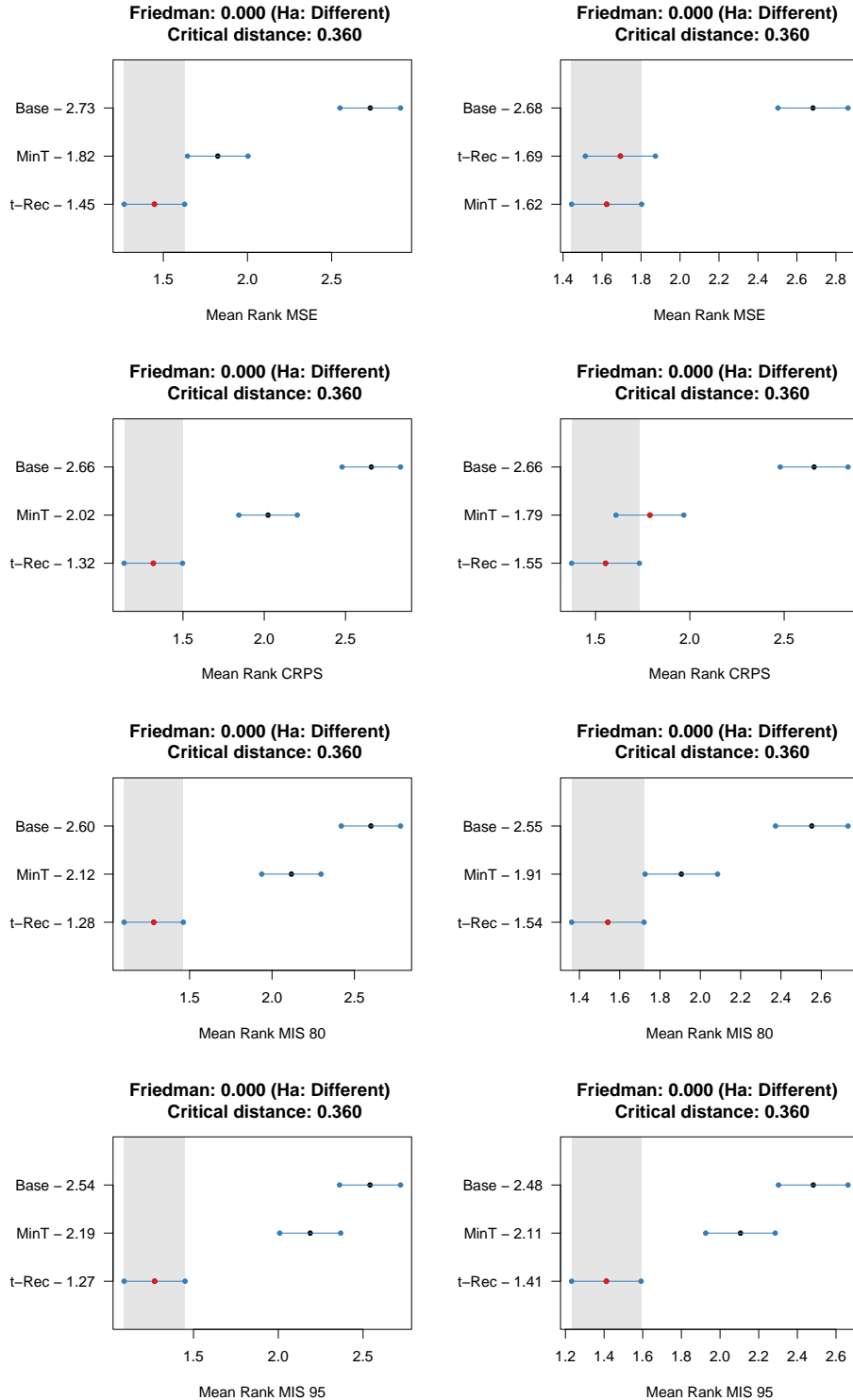


Figure C.13: Friedman and post-hoc Nemenyi tests results for the *Australian tourism-Q* dataset. The columns represent different choices of training length: 25 and 40 observations, respectively. The rows correspond to the metrics: the first row shows the MSE, the second row displays the CRPS, the third row presents the MIS calculated for the 80% prediction interval, and the fourth the MIS calculated for the 95% prediction interval.

Appendix D. Additional results on the diagonal prior scale parameter

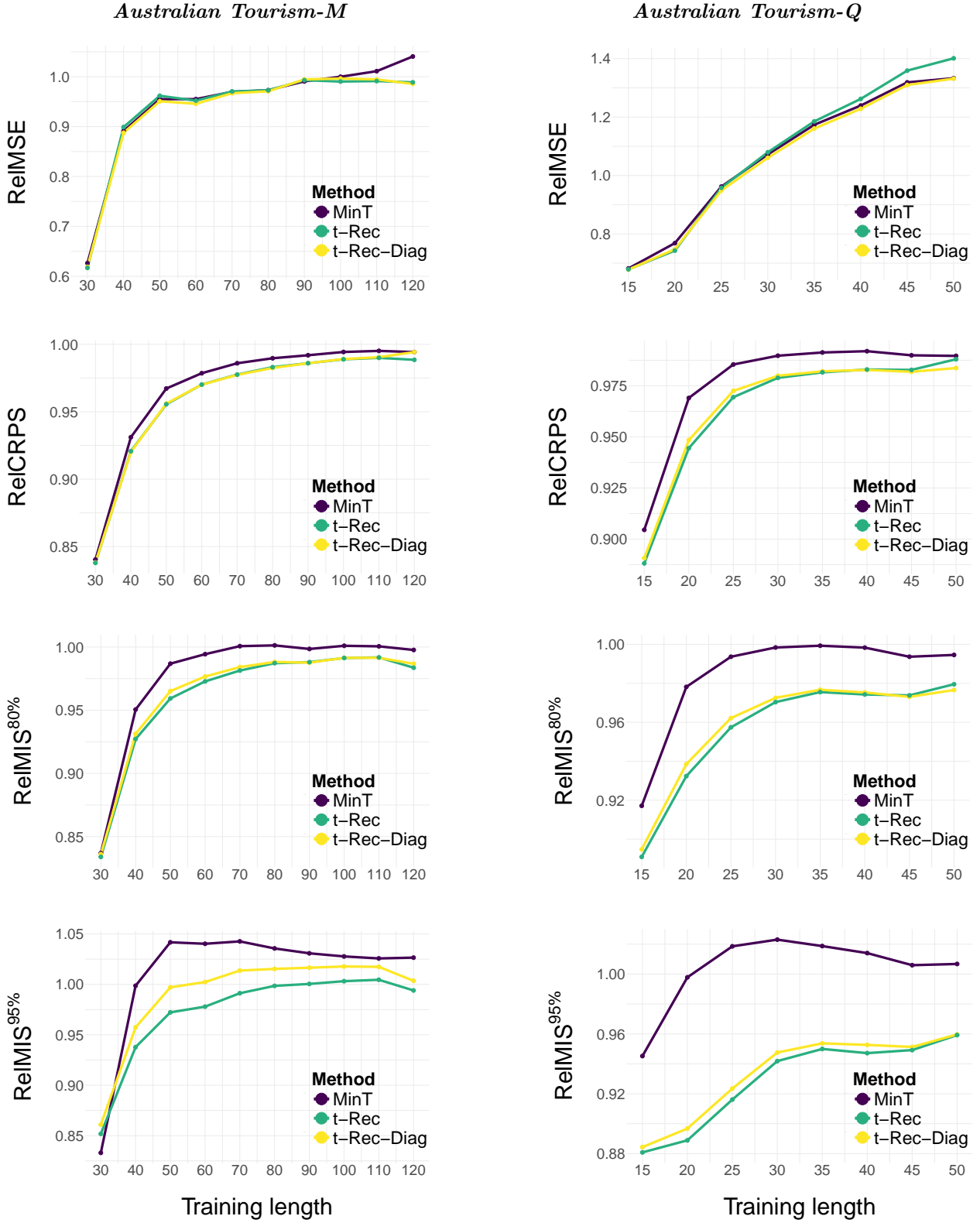


Figure D.14: Results on the *Australian Tourism-M* (left column) and *Australian Tourism-Q* (right column) datasets for *MinT* (purple), *t-Rec* (green) and *t-Rec-Diag* (yellow). A relative score lower than 1 means improvement over the base forecasts.